Photo-activation of ruthenium-decorated upconverting nanoparticles

Meijer, M.S.

CHAPTER 7

Summary, conclusions, and outlook

7.1 Summary

7.1.1 Near-infrared photo-activation of ruthenium phototherapy prodrugs

The last decades have seen a significant increase in the use of light as a non-invasive trigger for the activation of prodrugs in the treatment of cancer, improving the selectivity of cancer treatment by offering both spatial and temporal control over the drug activation. Photodynamic therapy (PDT) and photo-activated chemotherapy (PACT) are among the most promising treatment modalities in phototherapy. Despite a clear difference in their mode of action, the prodrugs for these two treatment modalities can be structurally very similar. Metal-based prodrugs based on ruthenium(II) polypyridyl complexes have proven to be especially suitable for application in both phototherapeutic techniques, due to their tuneable photochemical properties. As most ruthenium polypyridyl complexes unfortunately require poorly-penetrative, potentially-toxic blue light (400–500 nm) for their photo-activation, a lot of research effort has been dedicated to the development of prodrug systems that can be activated using light in the "phototherapeutic window" (600–1000 nm). Light in this spectral range is less harmful and penetrates deeper into human tissue. Thulium-doped upconverting nanoparticles (UCNPs) produce the desired blue light upon excitation in the phototherapeutic window, making them a promising candidate for a drug delivery system, in which ruthenium prodrugs can be activated with near-infrared light. Several groups have shown that it is possible to trigger the photosubstitution of monodentate ligands in ruthenium complexes using NIR light and UCNPs, paving the way for the development of near-infrared-driven PACT. The main goal of the research described in this thesis was to expand the UCNP-mediated photo-activation of ruthenium prodrugs to tris-bidentate ruthenium polypyridyl complexes for both PDT and PACT.

7.1.2 Upconversion quantum yield of blue-emitting UCNPs

As a result of the large, active community that works on their development of UCNPs, new optimizations appear continuously in the scientific literature. An essential parameter for the direct comparison of the optical properties of these systems is the internal upconversion quantum yield (Φ_{UC}), defined as the amount of upconverted photons emitted per photon absorbed. Unfortunately, the Φ_{UC} is rarely reported for UCNPs, as its determination often requires complex equipment and extensive technical expertise. In Chapter 2, we showed that determination of the Φ_{UC} is also possible using relatively simple and economical equipment. We

presented the first Φ_{UC} values for $LiYF_4:Yb^{3+},Tm^{3+}$ UCNPs, and, in the first multicentre absolute measurement of the Φ_{UC} of UCNPs, showed that our results were comparable to Φ_{UC} values obtained for the same batch of UCNPs in Karlsruhe and Berlin, using state-of-the-art setups. Importantly, we reported the Φ_{UC} for each of the individual visible and near-infrared upconversion emission bands in these UCNPs, which is relevant as their intensities are multiple orders of magnitude apart. Whereas the Φ_{UC} value of the main emission band, at 794 nm, is ~ 0.02 at an excitation power density of 5 $W \cdot cm^{-2}$, the blue emission band at 480 nm has a much lower quantum yield of ~ 6×10^{-5} under these conditions. We examined the power dependency of the Φ_{UC} of the various emission bands, and found that none of the visible emission bands showed signs of saturation up to 400 $W \cdot cm^{-2}$, whilst the excitation power density for phototherapeutic applications should be kept below 1 $W \cdot cm^{-2}$. Overall, the low efficiency of the blue upconverted emission in Tm-based UCNPs justifies the need for further material research aimed at increasing the upconversion quantum yields of UCNPs in the blue region of the spectrum, allowing for the more efficient application of these UCNPs in blue light-triggered phototherapy.

7.1.3 Light-driven ROS generation using ruthenium and lipid-coated UCNPs

In Chapter 3, we describe a method to render UCNPs water-dispersible, while simultaneously decorating their surface with ruthenium complexes, suitable for either PDT or PACT. This single-step strategy consisted of coating the surface of blue-emitting $NaYF_4:Yb^{3+},Tm^{3+}$ UCNPs with a mixture of phospholipids and amphiphilic ruthenium complexes. To this end, we designed two ruthenium complexes (Scheme 7.1, left), i.e. the photostable complex $[Ru(bpy)_2(bdophen)](PF_6)_2$ ($[\mathbf{1}](PF_6)_2$, bpy = 2,2′-bipyridine, bdophen = 5,6-bis(dodecyloxy)-1,10-phenanthroline) and the photolabile complex $[Ru(bpy)_2(bdodmphen)](PF_6)_2$ ($[\mathbf{2}](PF_6)_2$, bdodmphen = 5,6-bis(dodecyloxy)-2,9-dimethyl-1,10-phenanthroline). These were based on the well-known photosensitizer $[Ru(bpy)_3]^{2+}$ and its photolabile strained PACT analogue $[Ru(bpy)_2(dmbpy)]^{2+}$. Unfortunately, irradiation of $[\mathbf{2}](PF_6)_2$ with blue light leads to the unselective photosubstitution of a mixture of the bdodmphen ligand and one of the bpy ligands, making it unsuitable for use in combination with UCNPs. On the other hand, $[\mathbf{1}](PF_6)_2$ is a good photosensitizer for the generation of singlet oxygen. Application of phospholipids and $[\mathbf{1}]^{2+}$ to the surface of oleate-capped UCNPs resulted in the formation of a stable, negatively-charged nanoconjugate (UCNP@lipid/$[\mathbf{1}]^{2+}$), with $[\mathbf{1}]^{2+}$ located directly at the water-lipid interface of the

lipid bilayer, no more than 5 nm from the UCNP surface. Lifetime studies revealed that there is non-radiative energy transfer from one of the Tm^{3+} excited states to [**1**]$(PF_6)_2$, but that its efficiency is limited (12%). As the blue upconverted emission was reduced by more than 12 percent upon the addition of the ruthenium complex, we believe that radiative energy transfer also plays a role in the activation of [**1**]$(PF_6)_2$ by the UCNPs. Although the lack of a water-soluble, positively-charged, selective reactive-oxygen-species-detecting probe precluded the determination of the type of reactive oxygen species (ROS) produced in the membrane, we found that UCNP@lipid/[**1**]$^{2+}$ produces significant quantities of ROS under 969-nm irradiation, making it the first example of a ruthenium-based PDT prodrug activated using UCNPs. The ruthenium-decorated nanoparticles generated up to five times more ROS than particles that lacked the ruthenium complex.

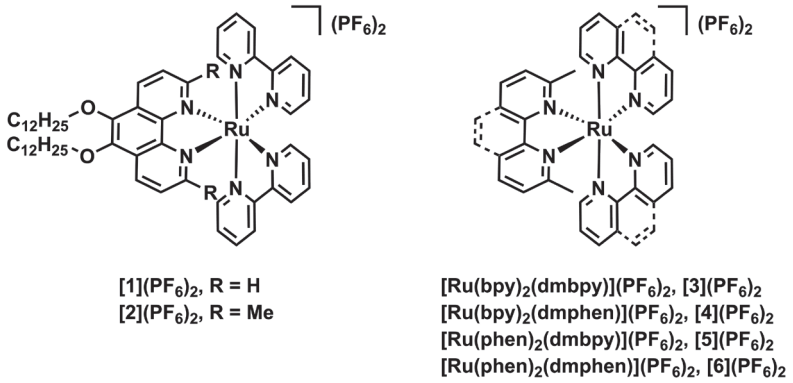

[1]$(PF_6)_2$, R = H
[2]$(PF_6)_2$, R = Me

[Ru(bpy)$_2$(dmbpy)]$(PF_6)_2$, [3]$(PF_6)_2$
[Ru(bpy)$_2$(dmphen)]$(PF_6)_2$, [4]$(PF_6)_2$
[Ru(phen)$_2$(dmbpy)]$(PF_6)_2$, [5]$(PF_6)_2$
[Ru(phen)$_2$(dmphen)]$(PF_6)_2$, [6]$(PF_6)_2$

Scheme 7.1. Chemical structures of the ruthenium complexes discussed in Chapters 3 and 4.

7.1.4 Ligand rigidity steers the selectivity and efficiency of photosubstitution

The non-selective nature of the photosubstitution reaction reported in Chapter 3 prompted us to investigate this phenomenon further, the results of which are described in Chapter 4. We hypothesized that the relative rigidity of the bidentate ligands may play a role in the selectivity and efficiency of photosubstitution reactions in this family of complexes. We synthesized four sterically-hindered ruthenium complexes of the general formula $[Ru(N\hat{}N)_2(dmN\hat{}N)](PF_6)_2$ (Scheme 7.1, right), in which N^N = bpy or 1,10-phenanthroline (phen), and dmN^N is either dmbpy or 2,9-dimethyl-1,10-phenanthroline (dmphen). These four complexes share very similar photophysical properties, as they all have an absorption maximum at 450 nm, and were all found to be photolabile, poorly emissive, and poor sensitizers for the generation of singlet oxygen. However, these

complexes differ in the rigidity of their ligands, as the phenanthroline-based ligands lack the rotational freedom that their bpy counterparts show upon dissociation of one of their nitrogen donors from the metal ion. Irradiation of all four complexes in solution results in the substitution of one of the bidentate ligands for two solvent molecules. The dimethylated ligand (dmN^N) is substituted selectively if it is not more rigid than the non-methylated ligands. On the other hand, for $[Ru(bpy)_2(dmphen)]^{2+}$ ($[\mathbf{4}]^{2+}$, see Scheme 7.1), where the dimethylated ligand (dmphen) is more rigid than the ancillary (bpy) ligands, we observed non-selective photosubstitution of either one of the three ligands, as reported for $[\mathbf{2}](PF_6)_2$ in Chapter 3. The photosubstitution quantum yield is to a large extent also regulated by the rigidity of the ligand being expelled, while that of the ancillary ligands plays virtually no role. The substitution of the more rigid dmphen ligand is up to two orders of magnitude less efficient than that of dmbpy. Despite the fact that photosubstitution in all four complexes is believed to proceed via a two-step mechanism, the overall quantum yields could all be fitted well with first-order rate equations, and we observed no spectral signature of the photochemical intermediate. For $[\mathbf{4}]^{2+}$, the ratio between bpy and dmphen substitution is dependent on the identity of the incoming ligand: the substitution of bpy is preferred if the complex is irradiated in acetonitrile, but the dmphen ligand is predominantly replaced in water/acetone mixtures. Furthermore, the efficiency of this photoreaction responds strongly to changes in the polarity of the reaction mixture, decreasing in rate with increasing polarity. Stabilization of the ^{3}MLCT excited state in the more polar water-rich media could be an explanation for this phenomenon, but more extensive computational work is necessary to provide a definitive answer.

7.1.5 Bisthioether ligands for selective and efficient photosubstitution

In our search for an anchoring bidentate ligand scaffold that can be selectively photosubstituted, we turned our attention to thioether ligands. Thioether sulfur atoms have been shown to form thermally stable, but photochemically labile coordination bonds with ruthenium(II) ions. In Chapter 5, we describe a novel, symmetric bidentate bisthioether ligand that bears a central alcohol functionality, available for covalent functionalization without the formation of regioisomers upon coordination of the ligand. Using this ligand, 1,3-bis(methylthio)-2-propanol, **7**, we synthesized the new ruthenium polypyridyl complex $[Ru(bpy)_2(\mathbf{7})](PF_6)_2$ ($[\mathbf{8}](PF_6)_2$, Scheme 7.2, left). Upon the coordination of ligand **7**, sixteen possible isomers can be formed, consisting of eight possible Λ diastereoisomers and their

Δ enantiomers. However, the synthesis proved to be diastereoselective, and we were able to determine which diastereoisomer had been obtained using 2D NMR and density functional theory (DFT) studies. The steric hindrance caused by the thiomethyl groups seems to be the main driving force for the formation of the isomer found. The alcohol group in the ligand is most likely oriented equatorially. Upon irradiation with blue light in water, the ruthenium complex selectively substitutes the bisthioether ligand in two steps. In contrast to the photosubstitution reactions described in Chapter 4, here we clearly observed the formation of a photochemical intermediate, as the second photochemical step is thirty times less efficient than the first step. We identified this intermediate species as the mono-thioether, mono-aqua complex. This relative stability of the intermediate species also allowed us to determine photochemical quantum yields for the individual reaction steps. Substitution of the alcohol group in the bisthioether ligand has no influence on the diastereoselectivity of the synthesis or the selectivity of the photosubstitution reaction, and only minor effects on the efficiency of these reactions were observed. We concluded that functionalized bisthioether ligands are promising candidates for use as photocleavable ligands for the binding of ruthenium-based PACT complexes to inorganic surfaces, such as that of UCNPs.

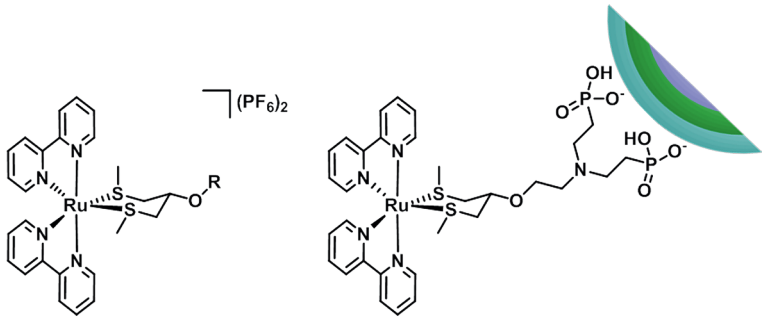

Scheme 7.2. Chemical structures of ruthenium complexes discussed in Chapters 5 and 6 and the structure of the UCNP nanoconjugate UCNP@[11] discussed in Chapter 6. Photo-irradiation of these complexes result in cleavage of the Ru–S bonds.

7.1.6 800-nm activation of a ruthenium bisthioether complex bound to core-shell UCNPs using phosphonate ligands

Finally, in Chapter 6, we report the modification of the abovementioned bisthioether ligand, and its ruthenium complex, with a spacer ending in two hard

anionic phosphonate moieties, forming complex [**11**]$(PF_6)_2$. This allows for anchoring of the complex to the surface of UCNPs, using a surface ligand exchange process (see Scheme 7.2, right). In comparison to Chapter 3, we also modified the type of UCNPs used, introducing two shell coatings on the outside of the Yb,Tm-doped core UCNPs. The first shell layer was doped with Nd^{3+}, to allow excitation of the particles with 796-nm light, thus avoiding the water heating often seen with excitation at 980 nm. The outer, undoped shell layer prevents surface quenching of the excitation, thus increasing the upconversion efficiency. Synthesis of the 41-nm diameter core-shell-shell UCNPs was performed through the injection of sacrificial nanoparticles, allowing for the formation of thin, isotropic shells. The phosphonate-modified ruthenium complex binds efficiently to the nanoparticle surface in neutral to slightly basic conditions (pH = 7.5–9.0), leading to the formation of a thermally stable nanoconjugate that is well dispersible in water. Under these conditions, where the phosphonate groups are fully deprotonated, up to 2.4×10^3 Ru(II) ions can be bound per UCNP. Irradiation of the UCNP@Ru nanosystem with either 796-nm or 969-nm light leads to photo-activation by photosubstitution, providing the first demonstration of the photo-activation of a ruthenium thioether complex using 796-nm irradiation of a water-dispersible nanoconjugate. Unfortunately, only partial release of the ruthenium photoproduct from the nanoparticle surface was observed after 6 hours at an excitation power density of 50 $W \cdot cm^{-2}$. This suggests that the efficiency of the photo-activation needs to be improved before this system can be applied in biology, for which the use of much shorter time scales (≤ 1 h) and lower excitation power densities (≤ 1 $W \cdot cm^{-2}$) is required.

7.2 Conclusions and outlook

7.2.1 UCNP surface coating for stability in aqueous media

In Chapters 3 and 6, we evaluated two methods for the stabilization of ruthenium-decorated UCNPs in aqueous media, namely encapsulation of the UCNP, together with its original oleate coating, in a phospholipid layer, or the replacement of the oleate coating by ruthenium complexes bearing zwitterionic bidentate phosphonate groups. At first glance, both methods appear to result in equally stable, water-dispersible nanoconjugates, and seem equally suitable for phototherapeutic applications. Examination of their hydrodynamic diameter by dynamic light scattering shows that both nanoparticle system predominantly exist as small 100-nm aggregates in aqueous dispersion. Also, a comparison of the

ruthenium-based absorbance in the UV-Vis absorbance spectra shows no clear difference in the ruthenium coating efficiency of the two systems. However, some differences between the systems can be found upon closer inspection. Generally speaking, sedimentation of the water-dispersible nanoparticles occurred faster for lipid-coated UCNPs than for the phosphonate-coated UCNPs, implying that the long-term stability may be lower for the lipid-coated UCNPs. Also, the extrusion procedure necessary to purify lipid-coated UCNPs is far more labour-intensive than the ligand-exchange procedure. On the other hand, the modular design of the lipid-coated system allows for easy modification of the lipid composition or exchange of the ruthenium complex used. Furthermore, the negative surface potential of the lipid-coated UCNPs, caused by the use of a large amount of DOPA phospholipid, is beneficial with respect to *in vivo* applications, compared to positively-charged UCNPs. Positively-charged nanoparticles are known to be non-selectively taken up by cells, whereas negatively-charged liposomes and polymersomes were recently shown to undergo selective uptake by liver endothelial cells. The undesired uptake by these cells can be suppressed by co-treatment with dextran sulfate, extending the circulation time of negatively-charged particles.[1]

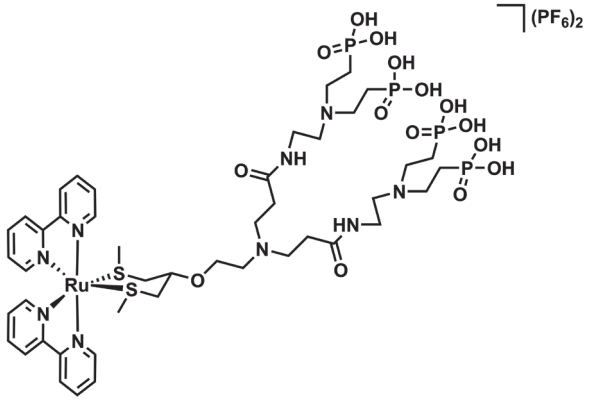

Scheme 7.3. Proposed photo-activatable ruthenium complex bearing a tetraphosphonate groups for the coating of UCNPs.

A factor that we have not studied, is the stability of the UCNP nanoconjugates in media or buffers that contain high concentrations of competitive UCNP-binding ions (e.g. phosphates). By increasing the denticity of the surface binding groups, the stability of the system in such buffers could be improved, as shown before by the group of Winnik, who used a PAMAM dendron modified with four

phosphonate groups.[2] Scheme 7.3 shows a ruthenium polypyridyl complex bearing a photocleavable ligand with such a tetraphosphonate group for UCNP binding.

7.2.2 Selecting ruthenium(II) complexes for UCNP-based applications

Several factors are important in the development of ruthenium(II) photochemical prodrugs that can be released from a drug delivery system through photosubstitution. A first necessity is selectivity over which ligand is photosubstituted. Notably, only substitution of the anchoring ligand will result in the release of the complex from the drug delivery system. In Chapter 3, we discussed the use of a sterically hindered ruthenium(II) polypyridyl complex as a UCNP-bound photoreleased prodrug for PACT. In this compound, $[Ru(bpy)_2(bdodmphen)]^{2+}$ ($[\mathbf{2}]^{2+}$ in Scheme 7.1), we employed a sterically demanding phenanthroline-based ligand as the anchoring ligand, expecting it to dissociate upon irradiation with visible light. Instead, we observed the non-selective release of a mixture of bdodmphen and the more flexible bpy ligands, making the complex unsuited for its intended use as a photoreleased prodrug. A more systematic study into the selectivity of the photosubstitution reaction in sterically hindered ruthenium(II) tris-bidentate complexes, described in Chapter 4, confirmed that the rigidity of the ligands is the main parameter that determines which ligand is photosubstituted. The less rigid dmbpy ligand could not only be photosubstituted more selectively, but also significantly faster than its rigid dmphen counterpart. For the future development of sterically hindered ruthenium complexes for use in nanoparticle-bound systems, it is essential to ensure that the anchoring ligand is less rigid than the ancillary ligands. Apart from the addition of steric hindrance, photolability can also be introduced in ruthenium(II) polypyridyl complexes by electronic means, through the introduction of poorly σ-donating ligands, such as thioethers. This was exploited in Chapter 5 and 6, where we discussed the use of bidentate bisthioethers as anchoring ligands for the binding of ruthenium photo-activatable complexes to the surface of UCNPs. These ligands were found to be selectively photosubstituted under irradiation with blue light, and further functionalization of these ligands does not negatively affect their photophysical properties.

A second factor to take into account is the efficiency of the photorelease from the nanoparticle surface, which is determined by the efficiency of the photosubstitution reaction itself (the photosubstitution quantum yield, Φ_λ) and the

spectral overlap between the nanoparticle emission and the ruthenium absorbance spectra. In Chapter 4, we showed that the photosubstitution of dmbpy for water in both $[Ru(bpy)_2(dmbpy)]^{2+}$ and $[Ru(phen)_2(dmbpy)]^{2+}$ was not only selective, but also efficient ($\Phi_{466} \approx 0.03$). Furthermore, the ^{1}MLCT absorption maximum in these complexes is found at ~ 450 nm, coinciding with the $^1D_2 \rightarrow {}^3F_4$ thulium emission band at 451 nm. In this light, it would be interesting to investigate the use of anchoring ligands based on dmbpy, whereby anchoring groups could be attached to the 4- and 4'-positions of the bipyridine. Also, the use of ancillary ligands with slightly extended aromatic systems could be advantageous, as this may lead to an increase of the molar absorptivity of the ruthenium complexes, and thus to a more efficient energy transfer from the nanoparticles. Nonetheless, in doing this care should be taken to not increase the lipophilicity of the complex too much, as this may hamper the aqueous solubility of the nanoparticle system and increase its dark toxicity.[3] Also, one should avoid the introduction of low-energy excited states that lie on the ligand (intraligand or π–π^* states), which may compete with population of the ^{3}MLCT and ^{3}MC states.[4] Examples of suitable ancillary ligands are shown in Scheme 7.4.

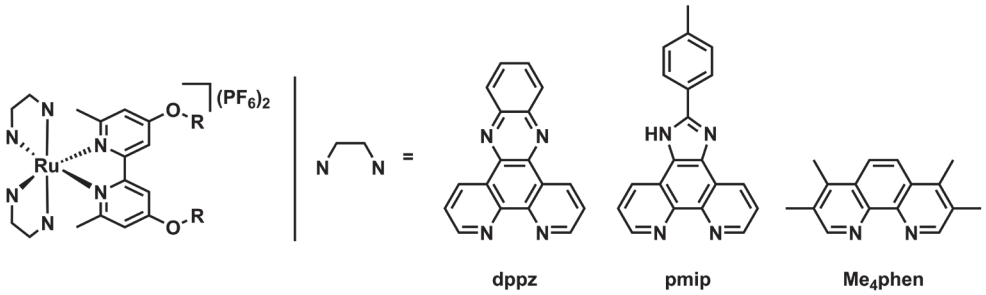

Scheme 7.4. Alternative strained polypyridyl ruthenium complexes, containing a dmbpy-based sterically demanding ligand to guarantee selective photosubstitution, and ancillary ligands with extended aromatic systems to increase the molar absorptivity of the complex.

The evaluation of the overall efficiency of photorelease for the bisthioether ligands described in Chapters 5 and 6 is complicated by the two-step nature of their photosubstitution reactions. Although the first step has a very high photosubstitution quantum yield ($\Phi_{445} \approx 0.12$–0.25), the second step is much slower, with Φ_{445} ranging from 0.0051 to 0.0093. The destabilization that causes the photolability of these bisthioether complexes also affects their ^{1}MLCT absorption bands, shifting its maximum towards higher energies (~ 415 nm), thus reducing the spectral overlap with the two blue thulium emission bands at 451 and 475 nm. Ultimately, this leads

to a limited photosubstitution efficiency under 796-nm irradiation, as reported in Chapter 6.

Recently, ruthenium polypyridyl complexes bearing photocleavable monodentate thioether ligands have been studied in our group.[5] These complexes, of the general structure $[Ru(tpy)(N^N)(SRR')]^{2+}$, where N^N is a bidentate polypyridyl ligand, typically show a ^{1}MLCT absorption maximum around 450 nm and photosubstitution quantum yields of 0.005–0.02, making them very suitable for activation by thulium-doped UCNPs. For example, Lameijer *et al.* showed that $[Ru(tpy)(dppz)(SRR')](PF_6)_2$, where SRR' is a thioether-glucose derivative, is a potent PACT prodrug.[6] Modification of the thioether ligand used in this study with a phosphonate anchoring group could transform this complex to a potent UCNP-activated PACT prodrug (Scheme 7.5).

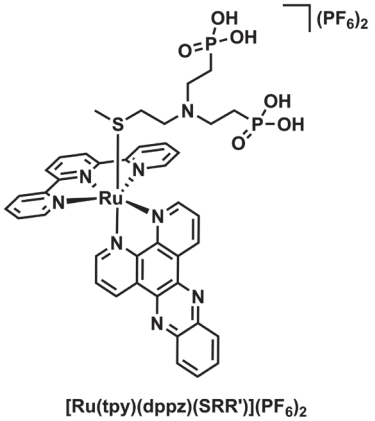

Scheme 7.5. Alternative ruthenium PACT prodrug bearing a photocleavable monodentate thioether ligand for UCNP binding.

7.2.3 UCNP selection for ruthenium activation: should we use Tm^{3+} or Er^{3+}?

As the ^{1}MLCT absorption maximum of ruthenium(II) polypyridyl complexes generally lies between 400 and 480 nm, most studies towards their activation with near-infrared light and UCNPs have been conducted using thulium-doped UCNPs.[7] However, in Chapter 2 we have shown that the blue emission bands of thulium are very weak, especially at the low excitation power densities that can be used in biological applications (≤ 1 W·cm^{-2}). Furthermore, in Chapter 6, we showed that the photo-activation of a bidentate bisthioether ruthenium complex bound to $NaYF_4$:Yb^{3+},Tm^{3+}@$NaYF_4$:Nd^{3+}@$NaYF_4$ core-shell UCNPs required extended irradiation times (6 h) at high excitation power densities (50 W·cm^{-2}). This leads us

to wonder whether it would be better to instead use Er-doped UCNPs for such applications, as these have been reported to have a higher upconversion quantum yield (Φ_{UC}).[8] However, the emission of the Tm^{3+} activator, with bands centred at 345, 365, 450, and 475 nm, obviously has a much better overlap with the ruthenium absorption bands than that of the Er^{3+} activator, which has its main emission bands at 520, 540, and 650 nm, along with a minor emission band at 410 nm. The question is whether the increased Φ_{UC} can make up for the reduction in spectral overlap between the erbium donor and the ruthenium acceptor.

Providing a general answer to this question is challenging, as the Φ_{UC} of UCNPs depends on several parameters, e.g. the size and surface functionalization of the particles, as well as the solvent, excitation power density, host lattice, dopant concentrations, and the possible core-shell structure of the particle. These parameters do not only influence the total upconversion quantum yield, but may also influence the relative intensities of the various emission bands that stem from different excited states. For example, as the Tm^{3+} emission bands at 450 and 475 nm are the result of 4- and 3-photon upconversion, respectively, an increase of the excitation power density would lead to an increase in the relative intensity of the 450-nm emission band. Despite these challenges, attempts can be undertaken to compare the efficacy of using thulium or erbium doping for a specific case.

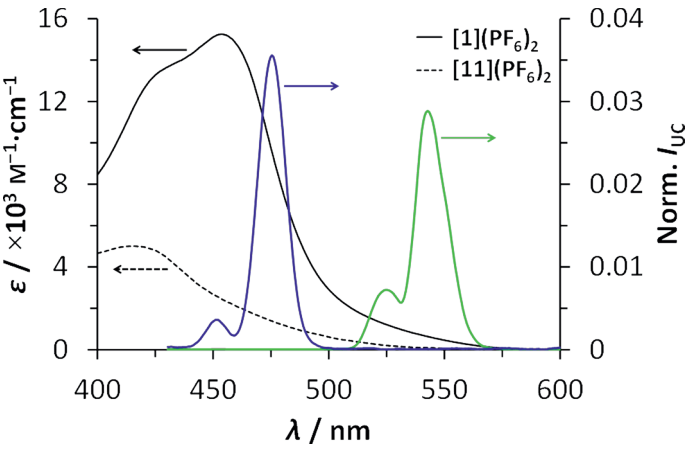

Figure 7.1. Estimated overlap between the emission bands of $NaYF_4:Yb^{3+},Tm^{3+}$ (blue) and $NaYF_4:Yb^{3+},Er^{3+}$ (green) on one hand, and the absorbance bands of ruthenium polypyridyl complexes $[1](PF_6)_2$ (solid black line) and $[11](PF_6)_2$ (dashed black line) on the other hand.

To this end, we define a system that employs ~ 40-nm diameter core $NaYF_4$ UCNPs doped with either ytterbium and thulium (20, 0.5%, as used in Chapter 3) or

ytterbium and erbium (18, 2%), irradiated in organic solvent under an excitation power density (P_{exc}) of 5 W·cm^{-2}. Firstly, we examine the spectral overlap between the emission of the two possible lanthanoid donors (Tm^{3+} and Er^{3+}) and the absorption of two potential ruthenium acceptors ([**1**]$(PF_6)_2$ shown in Scheme 7.1 and [**11**]$(PF_6)_2$ shown in Scheme 7.2). This spectral overlap can be quantified using the overlap integral $J(\lambda)$, defined by Equation 7.1.[9]

$$J(\lambda) = \int_0^\infty F_D(\lambda)\, \varepsilon_A(\lambda) \lambda^4 d\lambda \qquad \text{Equation (7.1)}$$

Here, $F_D(\lambda)$ is the emission intensity of the lanthanoid donor at each wavelength, normalized to the total emission in the wavelength area of interest, i.e. the 450 and 475 nm emission bands of Tm^{3+}, or the 520 and 540 nm emission bands of Er^{3+}, and $\varepsilon_A(\lambda)$ is the molar absorptivity of the acceptor at each wavelength. The spectral overlap of complex [**1**]$(PF_6)_2$ with the blue thulium emission bands (5×10^{14} M^{-1}·cm^{-1}·nm^4, Figure 7.1) is found to be almost an order of magnitude higher than with the green erbium emission bands (6×10^{13} M^{-1}·cm^{-1}·nm^4). A similar trend is found for the overlap with bisthioether complex [**11**]$(PF_6)_2$, showing an overlap of 7×10^{13} M^{-1}·cm^{-1}·nm^4 and 9×10^{12} M^{-1}·cm^{-1}·nm^4 with thulium and erbium emission, respectively (Figure 7.1).

Secondly, we looked at the efficiency of upconversion in Tm- and Er-doped UCNPs in organic solvent using P_{exc} = 5 W·cm^{-2}. In Chapter 2, we reported a $\Phi_{UC,blue}$ of 4.8–7.9 × 10^{-5} for the combined blue emission of 87×50-nm $LiYF_4$:Yb^{3+},Tm^{3+} UCNPs under precisely such conditions. Preliminary studies into the upconversion efficiency of their 44-nm diameter $NaYF_4$:Yb^{3+},Tm^{3+} counterparts used in Chapter 3 show that these are somewhat less efficient under these conditions, with a $\Phi_{UC,blue}$ of (3.3 ± 1.2) × 10^{-5} and a $\Phi_{UC,total}$ of 0.012 ± 0.004 (*data not shown*). A recent study showed that under the same conditions, the green emission quantum yield of 43-nm diameter $NaYF_4$:Yb^{3+},Er^{3+} UCNPs is around 5 × 10^{-4}.[8c] This is more or less an order of magnitude more intense than for the Tm-doped UCNPs. It thus seems that what we gain in emission intensity by using erbium donors, we may lose in terms of spectral overlap, making the use of both thulium and erbium emitters equally useful under the specified conditions. Which donor will ultimately result in a more efficient photo-activation of the ruthenium complex will depend on the precise quantum yield and overlap values of the system used, as well as several other parameters that govern energy transfer, e.g. the excited state lifetime and average *Ln*–Ru distance.

If we take the multiphotonic nature of the upconverted emission into account, and consider that saturation of these upconverted emission bands is not observed at biologically-relevant power densities, we can also hypothesize that the use of power densities much higher than 5 $W \cdot cm^{-2}$ will favour the use of the three- and four-photon blue Tm^{3+} emission bands, whereas the use of lower power densities will favour the use of the two-photon green Er^{3+} emission.

7.2.4 Efficient energy transfer from UCNPs to ruthenium acceptors

In Chapter 3, we have shown that the activation of the ruthenium PDT complex **[1]**$(PF_6)_2$ occurs at least partially via non-radiative energy transfer, i.e. via FRET with a FRET efficiency of 12%. Although this efficiency seems low, it is in line with values found for similar UCNP-based systems that use nanoparticles of a similar diameter.[10] The relatively low efficiency of non-radiative energy transfer in these systems can be explained by the large average distance between the donor atoms, equally distributed throughout the particle, and the acceptors on the surface. Only the lanthanoid ions close to the surface are able to participate in non-radiative energy transfer, whereas the majority of the ions is too far away from the surface, and can only transfer its energy radiatively, i.e. through emission and subsequent absorption by the acceptor.

The addition of active or inert shell layers to the outside of the UCNP, as shown in Chapter 6, increases the total upconversion quantum yield, leading to brighter emission from the thulium activators. However, these shell layers also increase the distance to the ruthenium complexes on the surface, thus strongly decreasing the likelihood of non-radiative energy transfer. Ultimately, there is a trade-off between upconversion efficiency and energy transfer efficiency, both via radiative and non-radiative pathways. Recently, some groups have investigated this trade-off by optimizing the efficiency of non-radiative energy transfer.[10-11] Although valuable, the ultimate goal, at least for UCNP-driven phototherapy, is the optimization of the activation of the surface-bound prodrug. For these applications, activation by radiative energy transfer is just as valuable as by non-radiative energy transfer, and Zhang *et al.* have shown that radiative energy transfer is responsible for the majority of activation events in most cases.[12] Nonetheless, both forms of energy transfer would benefit if it is possible to decrease the average donor-acceptor distance without hampering the brightness of the particles. The use of so-called onion-like nanoparticles, consisting of several layers with different dopant compositions could thus be advantageous (see Figure 7.2). The core layer could

consist of $NaNdF_4$, thereby maximizing the absorption of 800-nm light. A thin shell layer of $NaYF_4$:Yb^{3+} is responsible for transportation of excitons to the layer containing the activator, as well as preventing cross-relaxation between neodymium and the Tm^{3+} activator, which is present in the next layer ($NaYF_4$:Yb^{3+},Tm^{3+}). Finally, a thin inert shell layer prevents surface quenching by water. The shell layers contain somewhat smaller lanthanoid ions than the core, resulting in a slightly smaller host lattice unit cell, and in so-called tensile-strained shells, a benefit as these have been shown to yield more uniform epitaxial shell growth.[13]

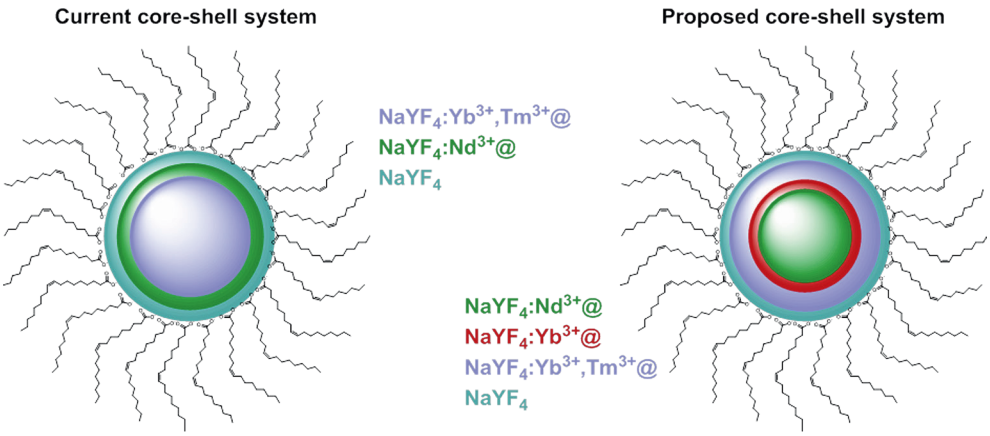

Figure 7.2. Current (Chapter 6) and newly proposed composition of core-shell UCNPs, reducing the average distance between the thulium activator ions and the ruthenium acceptor ions on the surface.

7.2.5 General conclusions

In this thesis, we have described the photo-activation of ruthenium polypyridyl complexes using near-infrared light and upconverting nanoparticles. We have shown that it is possible to generate water-dispersible, ruthenium-decorated upconverting nanoparticles from the as-synthesized, hydrophobic UCNPs in a single step by lipid encapsulation, or in two short steps using polar ruthenium complexes with anionic phosphonate groups that strongly bind to the nanoparticle surface. It is also shown that irradiation of the formed ruthenium-decorated UCNPs with NIR light at 796 or 969 nm leads to the activation of the ruthenium complexes, resulting in either the formation of reactive oxygen species (Chapter 3) or the release of the ruthenium photoproduct from the nanoparticle surface (Chapter 6). Notwithstanding, the relatively low efficiency of this photo-activation leaves room for improvement, with respect to the nanoparticles and the ruthenium

complexes used, and also with respect to the energy transfer between these components. This means that, in their current state, UCNP-based systems are still far from ready to be used in clinical phototherapy. However, through the work described in this thesis, we have gathered new insight into the design principles that are essential for the photo-activation of ruthenium-decorated upconverting nanoparticles, for which we have given suggestions.

7.3 References

[1] F. Campbell, F. L. Bos, S. Sieber, G. Arias-Alpizar, B. E. Koch, J. Huwyler, A. Kros, J. Bussmann, *ACS Nano* **2018**, *12*, 2138-2150.

[2] G. Zhao, L. Tong, P. Cao, M. Nitz, M. A. Winnik, *Langmuir* **2014**, *30*, 6980-6989.

[3] J.-A. Cuello-Garibo, M. S. Meijer, S. Bonnet, *Chem. Commun.* **2017**, *53*, 6768-6771.

[4] E. Wachter, E. C. Glazer, *J. Phys. Chem. A* **2014**, *118*, 10474-10486.

[5] a) R. E. Goldbach, I. Rodriguez-Garcia, J. H. van Lenthe, M. A. Siegler, S. Bonnet, *Chem. Eur. J.* **2011**, *17*, 9924-9929; b) A. Bahreman, B. Limburg, M. A. Siegler, E. Bouwman, S. Bonnet, *Inorg. Chem.* **2013**, *52*, 9456-9469.

[6] L. N. Lameijer, T. G. Brevé, V. H. S. van Rixel, S. H. C. Askes, M. A. Siegler, S. Bonnet, *Chem. Eur. J.* **2018**, *24*, 2709-2717.

[7] a) E. Ruggiero, C. Garino, J. C. Mareque-Rivas, A. Habtemariam, L. Salassa, *Chem. Eur. J.* **2016**, *22*, 2801-2811; b) Z. Chen, W. Sun, H.-J. Butt, S. Wu, *Chem. Eur. J.* **2015**, *21*, 9165-9170; c) Z. Chen, R. Thiramanas, M. Schwendy, C. Xie, S. H. Parekh, V. Mailänder, S. Wu, *Small* **2017**, *13*, 1700997; d) Y. Zhang, Z. Yu, J. Li, Y. Ao, J. Xue, Z. Zeng, X. Yang, T. T. Y. Tan, *ACS Nano* **2017**, *11*, 2846-2857.

[8] a) S. Fischer, J. K. Swabeck, A. P. Alivisatos, *J. Am. Chem. Soc.* **2017**, *139*, 12325-12332; b) C. Homann, L. Krukewitt, F. Frenzel, B. Grauel, C. Würth, U. Resch-Genger, M. Haase, *Angew. Chem., Int. Ed.* **2018**, *57*, 8765-8769; c) M. Kraft, C. Würth, V. Muhr, T. Hirsch, U. Resch-Genger, *Nano Res.* **2018**, *11*, 6360-6374.

[9] J. R. Lakowicz, in *Principles of Fluorescence Spectroscopy*, Springer US **2007**, p. 443-476.

[10] a) S. Melle, O. G. Calderón, M. Laurenti, D. Mendez-Gonzalez, A. Egatz-Gómez, E. López-Cabarcos, E. Cabrera-Granado, E. Díaz, J. Rubio-Retama, *J. Phys. Chem. C* **2018**, *122*, 18751-18758; b) V. Muhr, C. Würth, M. Kraft, M. Buchner, A. J. Baeumner, U. Resch-Genger, T. Hirsch, *Anal. Chem.* **2017**, *89*, 4868-4874.

[11] R. Marin, L. Labrador-Paéz, A. Skripka, P. Haro-González, A. Benayas, P. Canton, D. Jaque, F. Vetrone, *ACS Photonics* **2018**, *5*, 2261-2270.

[12] Y. Ding, F. Wu, Y. Zhang, X. Liu, E. M. L. D. de Jong, T. Gregorkiewicz, X. Hong, Y. Liu, M. C. G. Aalders, W. J. Buma, H. Zhang, *J. Phys. Chem. Lett.* **2015**, *6*, 2518-2523.

[13] N. J. J. Johnson, F. C. J. M. van Veggel, *ACS Nano* **2014**, *8*, 10517-10527.